Direct time-domain observation of laser pulse filaments in transparent media

H. Dachraoui,* C. Oberer, M. Michelswirth, and U. Heinzmann†
Molecular and Surface Physics, Faculty of Physics, Bielefeld University, D-33615 Bielefeld, Germany
(Received 25 March 2010; published 13 October 2010)

The interplay among self-focusing, energy depletion, and plasma formation is fundamental to the understanding of laser-matter interaction. In this article, we present the first direct time-resolved observations of the propagation of intense femtosecond laser pulses experiencing conical emission, self-focusing, self-guiding, beam filamentation, plasma defocusing, and continuum generation in wide-band-gap dielectrics. We demonstrate that continuum generation involves different mechanisms as a function of deposited energy.

DOI: 10.1103/PhysRevA.82.043820 PACS number(s): 42.65.Jx, 42.65.Sf, 42.65.Ky, 42.25.Bs

I. INTRODUCTION

The nonlinear propagation of intense laser radiation through transparent optical media is usually accompanied by many interesting effects. One example of these phenomena is the superbroadening of the pulse spectrum into a white-light continuum [1], commonly called a supercontinuum, which represents the strong modifications in the spatiotemporal properties of the laser pulse [2,3]. An ultrafast white-light continuum is widely used nowadays in many different applications, for example, optical parametric amplification [4], few-cycle pulse generation [5], light detection and ranging (LIDAR) [6,7], and time-resolved broadband absorption and excitation spectroscopy [8]. Despite its widespread use, understanding of the fundamental physics responsible for spectral broadening and self-transformation of the pulse shape is still incomplete, largely because they result from a complex chain of events. One of the first explanations of spectral broadening was based on the mechanism of standard self-phase modulation (SPM), which is due to the intensity-dependent refractive-index change [1]. The instantaneous frequency deviation ($\delta\omega(\tau) = -kz\partial\Delta(n)/\partial\tau$, where $\Delta(n)$ is the nonlinear contribution to the refractive index, τ is the pulse duration, z is the propagation coordinate, and k is the wave number) is symmetric relative to the peak of the pulse. Here, the phase shift and frequency spread increase with z. Continuum generation is always associated with self-focusing (SF), which leads to an explosive increase in the peak intensity and to the occurrence of other higher-order nonlinear optical processes. Therefore, the physical mechanisms that contribute to continuum generation can be complex. Many different possibilities have been proposed, in particular, SPM enhanced by self-steepening [9], four-wave mixing [10], SPM enhanced by SF [11], and ionization-enhanced SPM [12–14]. Furthermore, it has been shown that the generated free electrons cause spectral superbroadening on the blue side. In this scenario, the frequency deviation $\delta\omega$ is positive due to the negative contribution Δn_e to the refractive index from the free electrons, the density of which grows during the pulse. The spectral broadening is asymmetric and blue shifted relatively to the laser central frequency [12]. The free electrons' contribution to the negative change in the refractive index at frequency ω can be described by the Drude model [15]: $\Delta n_e \approx N_e e^2/\epsilon_0 m_e \omega^2$; where e and m_e are the charge and mass of the electron, N_e is the electron density, and ϵ_0 is the vacuum dielectric constant. At the same time the generated free electron has a defocusing effect by filament formation and contributes essentially to limiting the collapse of intense ultrashort pulses. The filamentation of the pulses is the result of dynamic competition between beam Kerr SF and defocusing caused by the plasma [16]. Besides plasma defocusing, and because of the associated broad spectral bandwidth, material dispersion alters the dynamics of collapse. For example, high dispersive effects lead to temporal splitting of the pulse into two symmetric subpulses and to the prevention of its collapse [17–19]. The collapse suppression is mainly attributed to group-velocity dispersion (GVD) and plasma defocusing, although in Ref. [20] a non-negligible role for multiphoton absorption (MPA) was suggested because of depletion of the laser beam. An important feature of continuum generation is the blue-red asymmetry. In addition to multiphoton ionization (MPI), it seems to be enhanced by self-steepening and space-time focusing [21–23].

For high-intensity laser pulses ($P > P_{\mathrm{cri}}$, the critical power for SF), the propagation is characterized by the breakup of the laser beam into distinct filaments [24,25]. Each small-scale filament can act as a source of the white light. Past work [25,26] has demonstrated the high degree of the special coherence between these transverse light sources. Interestingly, using femtosecond pulses at 1.5 μm, Saliminia *et al.* [27] have observed stable interference far-field patterns, where the deduced filament separation from their analysis is consistent with that directly measured. Moreover, it is shown that under certain conditions multiple filaments play a crucial role in the cutoff extension in the ultraviolet spectral region [28,29]. Several single-shot femtosecond laser studies of multiple foci processes into different media have correlated the generation of multiple filaments with both laser instability and spontaneous fluctuation of the refractive index in the media [24,30]. In this scenario, the primary filaments are generated from the initial perturbations randomly in the pulse cross section. The interference of their ring structures, appearing during defocusing in the laser-induced plasma, generates new centers of random initiation of secondary child filaments [31,32]. In addition, control of multiple filamentation patterns and the competition between them have been discussed in several articles [32,33].

*dachraoui@physik.uni-bielefeld.de
†uheinzm@physik.uni-bielefeld.de

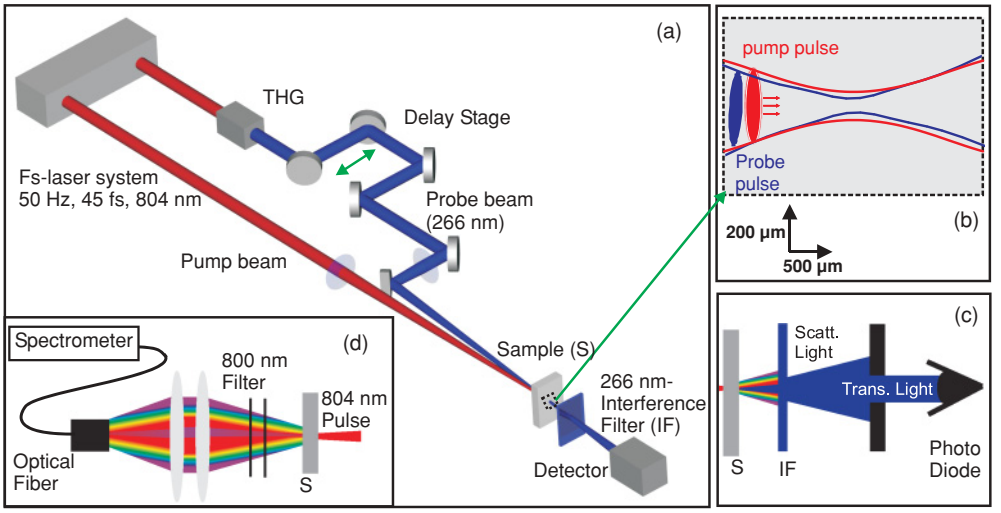

FIG. 1. (Color) (a) Schematic of the experimental setup to probe the propagation dynamics of intense femtosecond pulses in different transparent media. (b) Propagation of the pump and probe pulse in the absence of nonlinear effects. (c) Transient transmission geometry of the probe pulse and detection. (d) Experimental setup for measuring the white-light continuum spectra.

In this article, we report time-resolved studies of the mechanisms that govern the propagation of intense femtosecond laser pulse in wide-band-gap dielectrics (fused silica and LiF crystal). We used an uv (266 nm) pulse to follow the spatiotemporal evolution of an 800-nm pump pulse experiencing SF, conical emission, splitting, beam filamentation, and continuum generation. We demonstrate that continuum generation involves different mechanisms as a function of deposited energy. We identify different regimes of the continuum generation, revealing the interplay among SF, MPA, and plasma defocusing. In particular, in the low-energy regime, supercontinuum can result from a four-wave interaction mechanism. Spectral superbroadening and strong blue-red asymmetry are triggered by the occurrence of the SF feature. High conversion efficiencies are observed when the pulses undergo multiple filamentation. Furthermore, our experimental results provide clear evidence that the interference of the supercontinuum spectral components arises in the course of multiple filamentation in an intense laser pulse and that the cutoff is limited by intensity clamping inside the filaments.

II. EXPERIMENTAL SETUP

A schematic overview of our experimental setup is shown in Fig. 1. An amplified titanium-sapphire femtosecond laser producing 10-mJ, 804-nm linearly polarized pulses at a repetition rate of 50 Hz and with a duration of 45 fs is used to generate the ir pump and uv probe beams (266 nm generated by frequency tripling): the ir pulse is used to generate white-light continuum in condensed media and the uv pulse is used to monitor the evolution of the sample. The temporal width of the third-harmonic pulse is estimated to be approximately 120 ± 20 fs (measured with a transient grating method). The diameter of the pump and probe beams before focusing are 2 and 0.5 cm, respectively. The pump pulse is focused to a spot diameter of about 120 μm ($1/e^2$) using a 50-cm focal length fused silica lens. The uv probe beam is directed through a variable optical-delay line before it is focused to a spot size of 60 ± 10 μm ($1/e^2$) using a $f = 30$ cm fused silica lens and directed to the central fraction of the interaction region within the dielectric medium with an angle of 3° with respect to the surface normal. In our experiment the used pump pulse energies are in the range of 5–250 μJ to give intensities between 1 and 50 TW/cm^2 if the focus is in vacuum. The intensity of the probe pulse is kept below the SF threshold (peak intensity $I \approx 0.1$ TW/cm^2; assuming the propagation in vacuum). In the absence of the pump pulse, the propagation of the probe pulse is not affected by SF and SPM. Behind the sample, the directly transmitted pump beam and the generated white-light continuum are filtered by use of an interference filter. In addition to this interference filtering, a diachronic mirror positioned behind the filter is used to reflect the probe pulses and pass the remaining fractions of the pump pulse and white-light continuum. The transmitted uv beam is detected either with a photo diode or a CCD camera. These experiments are performed on three dielectric samples: LiF (length = 2 mm; $E_{gap} = +11.8$ eV) and two fused silica samples with two different band gaps, silica 1 (length = 3 mm; $E_{gap} = 7.5$ eV) and silica 2 (length = 2 mm; $E_{gap} = 5.8 \pm 0.8$ eV). Silica 2 is optically transparent to wavelengths in the range of 180–260 nm (*its exact* E_{gap} *is unknown*).

The white-light continuum spectra are measured by a fiber-coupled spectrometer (Ocean Optics) covering the range of 1000–200 nm.

III. RESULTS AND DISCUSSION

A. Pulse propagation and continuum generation in low-intensity regime

The time evolution of the directly transmitted intensity of the probe pulse is shown in Fig. 2. In order to better determine the zero time delays between pump and probe pulses, we also include in Fig. 2 simulated cross correlations of mid-ir pump and 266-nm probe pulses. Zero time delay corresponds to

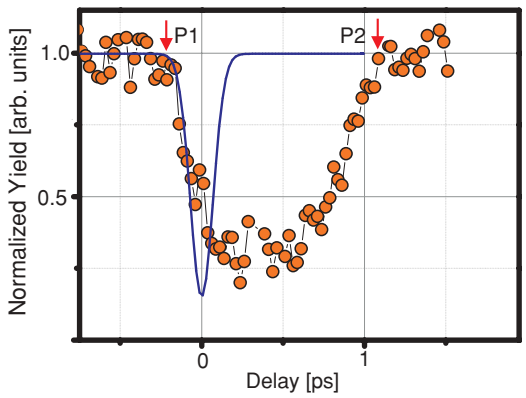

FIG. 2. (Color) Sample 1: Normalized 266-nm transmitted intensity versus pump-probe delay time; pump peak intensity $I = 5$ TW/cm^2. The solid line is a simulated cross correlation of the ir and 266 nm. The arrows serve to indicate the positions of the inflection points P1 and P2.

the moment where pump and probe pulses reach the center of the sample. Positive time delay corresponds to the ir pump preceding the probe pulse. Around zero delay time, when pump and probe overlap in time, the prompt reduction of the reconstructed transmission can be attributed to the pump-induced Kerr effect. At positive time delay $\tau > 300$ fs the transmission changes of the probe pulses can be assigned to the lifetime of the pump-induced free electron inside the plasma channel. The free carriers relax within several hundreds of femtosecond after the excitation, which is in good agreement with previous optical measurements on fused silica [34].

Figure 3 displays the intensity distribution of the far-field transmitted probe beam (out of sample 1), for various time delays between the ir pump and uv probe pulses and at two different laser pump energies. As we will see, the temporal evolution in the uv-beam profile can reflect the spatiotemporal properties of the pump pulse filament during the propagation. Despite the adopted precautions to block the directly transmitted pump beam and the white-light continuum, an undesirable

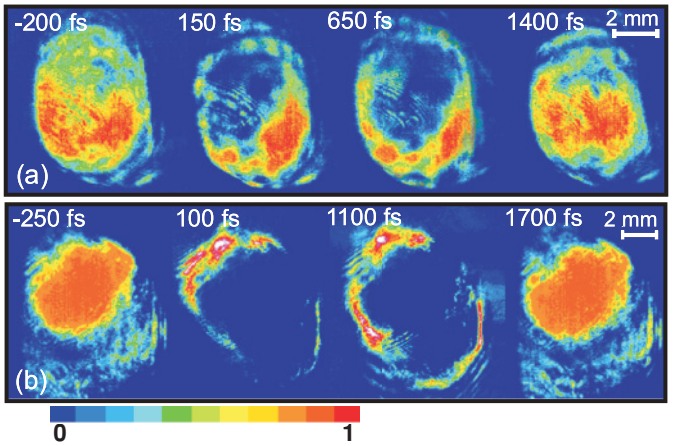

FIG. 3. (Color) Far-field image of the probe beam (266 nm) monitoring the evolution of the pump pulse filaments inside the silica 1 for two different input laser peak intensities. The pictures (a) and (b) represent the regime where SF is balanced by plasma defocusing. The corresponding intensity is 7 and 8 TW/cm^2, respectively.

background is observed. This background is subsequently subtracted from the presented pictures.

For laser energy smaller than 1 TW/cm^2, no change in the probe spot is noticed. Increasing the peak intensity of the pump pulse to 7 TW/cm^2, the probe spot begins to transform into a characteristic light ring structure [Fig. 3(a)]: a dark corona appears in the center of the uv spot. As mentioned earlier, around zero time delay, the origin of these observed transient changes is a pump-induced Kerr effect. At positive time delay $\tau > 300$ fs, the observed transient pattern represents the changes of the probe pulse due to the generation of free carriers. The bright ring around the corona develops synchronously with the corona rising. These observations provide clear evidence of the buildup of conical scattering (CS). The occurrence of this CS is better visualized in Fig. 3(b) (8 TW/cm^2), where the different uv spots with respect to the one at zero time delay are represented. Here, we repeated the measurements for a large opening angle of the probe beam with respect to the pump beam. Because of the beams' geometry, the symmetric ring of the scattered light transforms into two characteristic bright rings. The diameter of these rings changes with the readout angle. The onset of CS indicates that we are at the threshold for filamentation [35]. Due to the relatively small electron density in the filament, only a narrow white light is observed with naked eye. At time delay around 1400 fs the uv beam profile is similar to that from the unpumped case [Fig. 3(a)]. We measure the transmitted spectrum showing that there is spectral broadening. Since SF and SPM are related phenomena, this is a direct observation that SF does not occur. We will return to this point later.

As mentioned previously, white-light supercontinuum spectra essentially result from the spatial and spectral transformation of the initial pulse during nonlinear propagation inside the medium. Figures 4(a)–4(c) show typical white-light continuum spectra of various samples (sample 1, sample 2, LiF) obtained with 804-nm radiation focused at different peak intensities. Analyzing the recorded white-light continuum spectra in the energy range 5 TW/cm^2 $< I <$ 10 TW/cm^2 [green (bottom) curve] reveals that samples 2 and 3 have a nearly symmetric spectrum. While the spectrum of sample 1 exhibits a small red-blue asymmetry. As is mentioned previously, in this intensity range SF is not observed even when the SF threshold is nominally exceeded. This is the evidence for self-limitation caused by nonlinear absorption. MPA comes into play and lowers the peak intensity that can be reached. Thus, the intensity is too small to start MPI mechanisms. Recently, it has been demonstrated that MPA can be used to control the deposited energy in transparent media [20]. The observed slight broadening in this regime can be due to the fact that self-steepening occurs after MPI becomes active. Two fundamental questions remain unanswered: Which broadening mechanisms are responsible for continuum generation? Further, what is the origin of the conical scattering observed in Fig. 3?

In this intensity range, an explanation of the observed spectral broadening in terms of SPM associated with SF [11,19] can be ruled out for the following two reasons: (i) Figs. 3(a) and 3(b) do not exhibit SF features; (ii) in Fig. 4(d), there is no evidence for the existence of continuum band-gap dependence. In the SF stage, the continuum

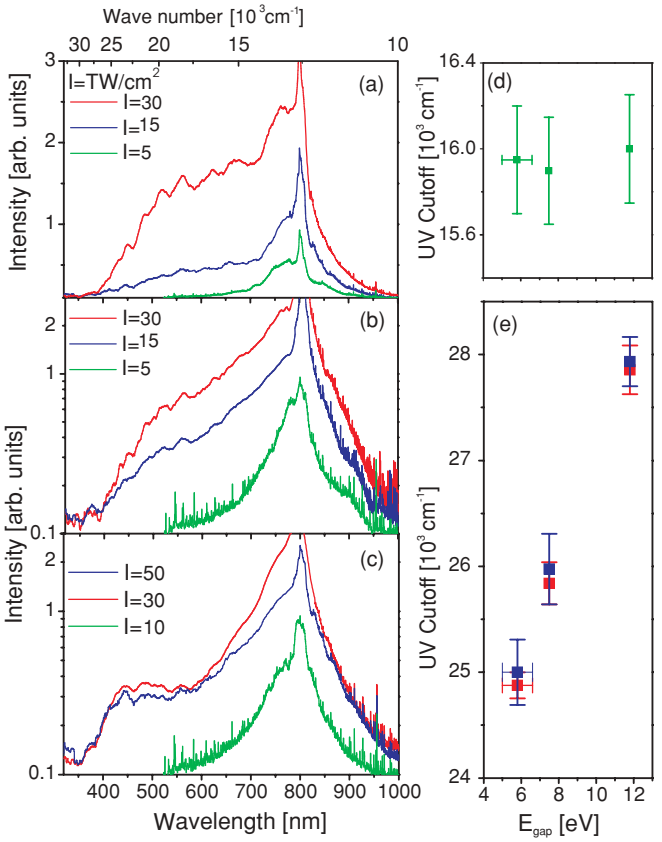

FIG. 4. (Color) White-light continuum spectra generated in sample 1 (a), sample 2 (b), and LiF (c) at different peak intensities. The green (bottom), blue (middle), and red (top) curves represent the situations observed in Figs. 3, 6, and 7, respectively. The obtained uv cutoffs are plotted for the three different regimes as a function of the band gap: (d) the green curves; (e) the blue and red squares correspond to the blue and red curves, respectively.

broadening increases with the rising of the band gap [36]. Here we propose the following scenario to explain the conical scattering and spectral broadening in this stage: Because the threshold for SF is clearly exceeded, we assume that SF comes into play and increases the intensity up to the self-limiting threshold, which is predicted at 10 TW/cm^2 in Ref. [20]. Thus, before the beam reaches its self-focus, MPA occurs and introduces the peak intensity, which would otherwise grow as it approaches the focus. This complex interplay leads to the compensation of SF by free-electron generation. So SF appears for a small time window before it is again balanced by defocusing caused by the plasma near the axis [21]. Once this condition is established the laser intensity is kept constant at slightly below the ionization threshold. We verified the assumption by determining the peak intensity under these conditions. A crude estimation of the filament size can be made by comparing the spot at time delay zero with that at 150 fs [Fig. 3(a)]. An input peak intensity of 7 TW/cm^2 gives a filament whose size ranges between 60 and 80 μm, which corresponds to maximum intensities of the order of 10 TW/cm^2. The balance between the self-focusing and plasma defocusing is characteristic for the formation of a long-living solitonlike waveguide [21,37]. The self-guiding mechanism is principally correlated with

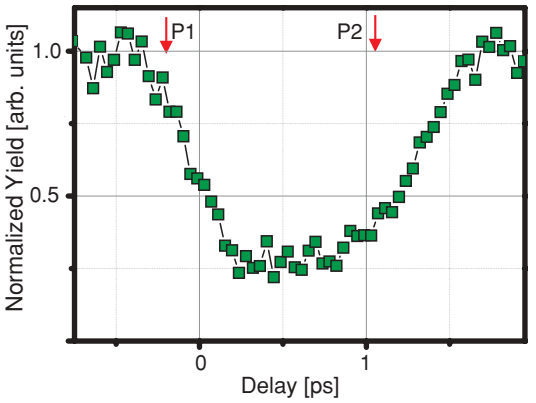

FIG. 5. (Color) Sample 1: Normalized 266 nm directly transmitted intensity versus pump-probe delay time; pump peak intensity $I = 25$ TW/cm^2. The arrows serve to indicate the positions of the inflection points P1 and P2 in the previous case.

conical emission. In this sense the conical scattering can be interpreted as the result of four-wave mixing during continuum generation in the medium. In addition to that, arguments can be found in the literature that link conical emission to four-wave mixing [38–40]. Our experimental data show that self-guiding actually results from the balance between self-focusing and free electrons.

B. Pulse propagation and continuum generation in strong transient focusing

We increased the pump peak intensity up to 10 TW/cm^2 to push these results further. Figure 5 displays the temporal evolution of the directly transmitted uv light in the pump intensity range 10 TW/cm^2 $< I <$ 25 TW/cm^2. The signal becomes much broader compared with the previous case, indicating the shifts of the inflection points P1 and P2. The negative (positive) shifts of P1 and P2 at the front (back) side of the curve are about -200 and 600 fs, respectively. Here, the negative shift of the front side is due to the decrease of the SF length with increasing the input intensity. The SF length is given approximately by $d_{\mathrm{SF}} = 0.367ka_0^2/[(\sqrt{P/P_{\mathrm{cri}} - 0.852})^2 - 0.0219]^{1/2}$ [41], where $k = 2\pi/\lambda$ is the wave number, a_0 is the spot size of the pump beam, and P is the pump power. In this case, the filament starts earlier along the propagation axis compared to the previous case. This observation is consistent with the moving-focus model. As mentioned previously, P2 mirrors the lifetime of the pump-induced free electrons. It is well known that the higher the excitation density, the faster the recovery process [42,43]: Due to the rising of the free-electron density and the electron-electron scattering rates, the free electrons relax more rapidly. A possible explanation of the unexpected subsequent behavior of the signal is the generation of secondary electrons (which becomes efficient after a certain energy level).

Characteristic time resolved intensity distributions of the far-field transmitted probe beam are shown in Fig. 6(a) (10 TW/cm^2 $< I <$ 16 TW/cm^2). In this regime, the situation is completely different from the previous case. A new feature begins to appear: the uv beam diameter is decreased compared with that of negative time delay, indicating that the Kerr-lens

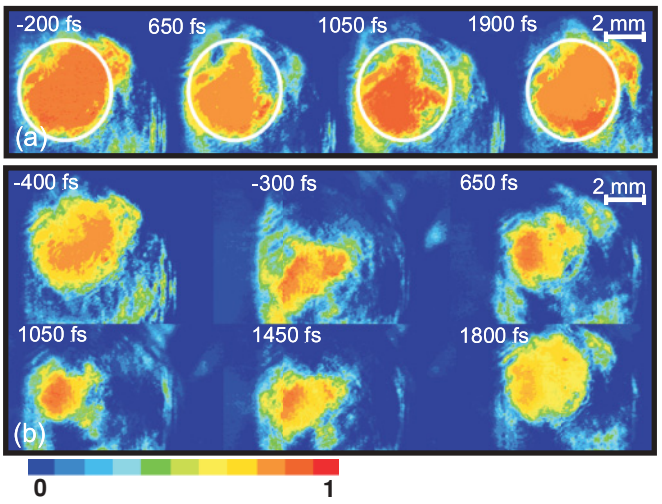

FIG. 6. (Color) (Sample 1) Time-resolved far-field spatial profiles of the 266-nm beam obtained for two different pump peak intensities: (a) $I = 15$ TW/cm^2 and (b) $I = 20$ TW/cm^2. The transient changes in (a) and (b) begin to appear at different time delays around 650 and -300 fs, respectively. The white contours indicate the position and the area of the initial state where the probe pulse reaches the sample before the arrival of the pump pulse.

effect comes into play and that the critical power P_{cri} for SF is exceeded. The critical power is a threshold power that causes SF and is given by $P_{\mathrm{cri}} = 3.77\lambda^2/8\pi n_0 \Delta n$, where n_0 and Δn are linear and nonlinear refractive indices of the medium, respectively. The occurrence of SF is strongly influenced by the interplay between different processes (MPI, MPA, etc.). This makes it difficult to determine experimentally the exact threshold for the occurrence of SF. The laser pump pulse is now intense enough to push the sample to act like a focusing lens. The passage from the geometric linear focal diameter to the self focal diameter causes a drastic increase in pump peak intensity, which leads to strong filament formation. In addition to that the relatively long rise time and lifetime now represent a distinct signature from the starting of another process, which is responsible for white-light continuum generation in this regime. At a time delay of about 2000 fs, the uv intensity profile resembles that from the unpumped case.

The situation is more clear at laser pump intensities of around 20 TW/cm^2 [Fig. 6(b)]. A dramatic decrease in the uv beam diameter is observed, indicting that the probe pulse undergoes a critical refocusing event. This observation indicates that the formation of an intense electron plasma channel and that of the fundamental pulse undergo a strong filamentation. In this regime the transient change occurs at an earlier time delay compared with the previous case. This observation is consistent with the moving-focus model: Increasing the input peak power leads to a filament that starts earlier along the propagation axis. The observed decrease at time delay $\tau = -300$ fs (when pump and probe pulses overlap in time) can be attributed to the pump-induced Kerr effect, whereas the origin of the apparent transient change at $\tau = 650$ fs is the pump-induced free carriers. In the last case a decrease by a factor 2 of the refocused diameter is estimated. The fact that the maximum reduction is observed at large time delays ($\tau > 300$ fs) is a clear signature of the contribution of the probe pulse to plasma generation. In this scenario the diameter of the probe beam undergoes a dramatic decrease inside the pump-induced plasma channel. A strong increase of the peak intensity follows, leading to the contribution of the probe pulse to the plasma generation and the occurrence of the Kerr effect (probe pulse). Indeed, these observed different transient changes reflect the interplay between the different processes involved in the generation of a white-light continuum.

More information about these observations can be delivered by inspecting the different spectra. For sample 1, the blue (middle) curve in Fig. 4(a) illustrates the output white-light spectrum in this regime. As can be seen, the length of the nonlinear interaction in the filament is long enough to transform the essential part of the input pulse energy into a wide range of spectral frequencies. The white-light continuum is characterized by a dramatic spectral broadening toward the shorter wavelengths. It is well known that large band-gap materials tend to show such asymmetric broadening in the anti-Stokes side of the spectrum [41]. For sample 2, increasing the pump intensity leads to the formation of a broadband emission between 500 and 800 nm characterized by high conversion efficiency. The continuum extends continuously from the pump wavelength in the uv spectral region and exhibits a cutoff around 500 nm. The situation differs in principle for the LiF sample; the extension of the continuum is marked by a drop in the conversion efficiency around 600 nm. The spectral intensity in the plateau region decreases to 10% of the peak intensity. Despite this dramatic drop the continuum exhibits a broadband plateau and a uv sharp cutoff around 400 nm. In this regime, the SF develops a high asymmetric pulse shape, where the trailing portion of the pulse is enhanced, resulting in a broad blue-shifted spectrum [17]. It further enhances the Stokes–anti-Stokes asymmetrical self-steepening of the pulse which eventually extends the continuum into the uv spectral region. On the other hand, Brodeur and Chin [14] interpret the large spectral broadening on the anti-Stokes side by introducing MPI in a moving-focus model. Such a connection was proposed first by Bloembergen [12] to explain the picosecond continuum.

In the strong SF regime, the cutoff is further extended into the uv region with increasing the band gap, as shown in Fig. 4(e). These observations are in good agreement with the data of Ref. [36]. The authors proposed to explain the correlation between SF and the band gap depending on a mechanism that involves free-electron generation in continuum generation: SPM is enhanced by MPE. Our data show that high conversion efficiency and strong Stokes–anti-Stokes asymmetry are triggered by the onset of catastrophic SF. Thus, the large blue shift is characteristic for SPM enhanced by self-steepening as well as by space-time focusing effects during the pump pulse filamentation [9,22]. Our data are consistent with the numerical results, which correlate large blue spectral broadening with taking into account the space-time focusing as well as self-steepening.

C. Propagation and continuum generation in multiple-filament regime

At increasing excitation energies, a strong background tends to blur the transmitted 266-nm probe light. This case

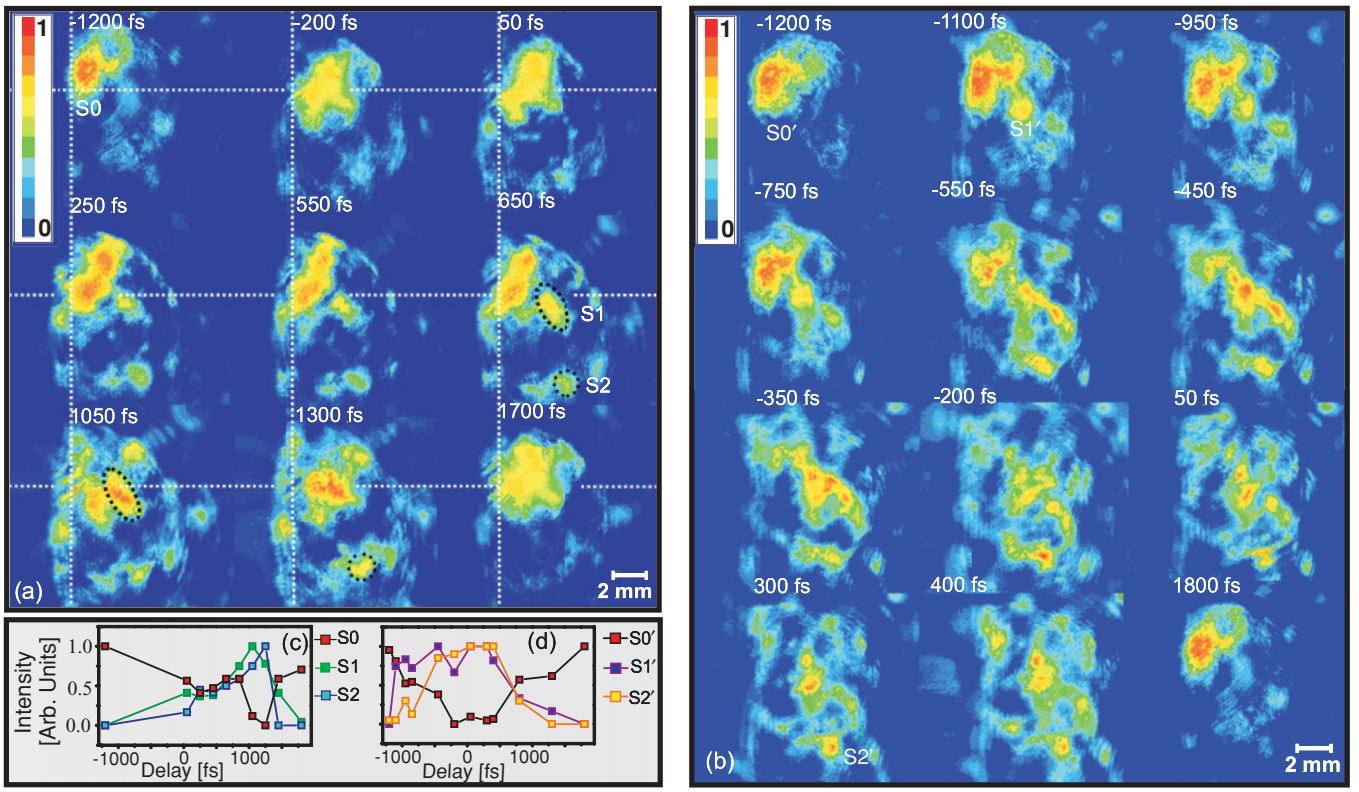

FIG. 7. (Color) (Sample 1) Far-field image of the 266-nm beam as a function of the pump-probe delay obtained for two pump intensities: (a) $I = 30$ TW/cm^2 and (b) $I = 50$ TW/cm^2. The curves in (c) and (d) show the temporal evolution of the primary and secondary filaments: (S0, S0′) parental, (S1, S1′) first generation of children, and (S2, S2′) second generation filaments' children.

is presented in Fig. 7(a). Here, only a small fraction of the directly transmitted uv light can be distinguished from the strong background. In this intensity range (25 TW/cm^2 $< I <$ 50 TW/cm^2) a further new feature begins to appear: multiple refocused spots occur after the excitation and spatially develop around the principal spot. The buildup of these different spots occurs at different time delays. Before describing this pattern more in detail, let us first examine the origin of the temporal broadening of the observed transient changes. An increase of the free electrons' lifetime is the most plausible explanation of this subsequent recovery: the generation of secondary electrons. The transient changes begin to appear at a negative time delay around -200 fs (filamentation starts earlier). For time delays after the temporal overlap (between probe and pump), the propagation of the probe pulse is strongly dependent on the dynamics of the pump-induced free carriers' density. High electron density leads to the occurrence of probe Kerr nonlinearity and to the contribution of probe pulse to the plasma generation. Here the observed complicated patterns probably arise from the probe-induced multiple filament generation, due to its decrease in diameter inside the pump-created plasma channel. At time delay $\tau \approx 250$ fs, the principal filament begins to decompose into two filaments, around which ring structures caused by the scattering in the laser plasma are formed. The two systems of rings begin to interfere with each other leading to the initiation of a child filament around $\tau \approx 650$ fs. At time delays around $\tau \approx 1050$ fs, the pump free carriers' density reaches its maxima leading to the occurrence of a further step toward the multifilament formation: interference of waves, resulting for primary and secondary filaments, which generates further regular centers of child filaments. Because of energy limitation, competition between the parental and child filaments occurs. The result of this competition is the disappearance of the primary filaments. The spatial separation of transverse filaments S1 and S2 in the center of the sample can only be roughly estimated to be about 60 μm. At subsequent delays (1700 fs), the uv beam profile is relatively similar to that of the initial case. Here, we notice that a combination between intensity perturbations of the probe pulse and strong fluctuations of the refractive index in the medium is the origin of the observed multifilamentation. Our experimental data are consistent with the numerical simulation of Hosseini *et al.* [32]. On the basis of these observations, it can be deduced that a continuum is generated along each filament, and in each filament the super continuum sources are created. The phase shifts between the same spectral components generated by different sources depend on the source position in both longitudinal and transverse directions. The high degree of the special coherence between the transverse light sources was demonstrated in a previous study [27].

As we can see, in Figure 7(b), when the laser pulse energy is further increased and is just below the level required for material breakdown (50 TW/cm^2) [44], the transient change starts at an earlier time delay as predicted by the moving-focus model: the filamentation starts before the geometric focus. In the time delay interval (-1200 fs $< \tau < -1000$ fs), when the pump and probe pulse overlap in time, multiple refocused spots are observed due to the multifilamentation of the pump pulse.

For a large time delay, the rising of the probe peak intensity, due its decrease in diameter inside the primary filaments, leads to the generation of further filaments: self-multifilamentation of the probe pulse. An example of the energy transfer between primary and secondary filaments is illustrated at a time delay of −750 fs. Due to the constructive interference between S0′ and S1′ the intensity in the overlapping region becomes larger. This leads to a larger refractive index in the center due to the Kerr effect. The energy of the parental filament is attracted toward the center, resulting in a new filament S2′ and the disappearance of S0′. The enhancement of the filament's number leads to the rising of the dispersed energy outside: defocusing by the induced plasma. One can see that there is no significant difference between the uv intensity profiles at time delays of −1200 and +1800 fs. A principal conclusion can immediately be derived that white-light filamentation is affected by various nonlinear phenomena depending on the deposited energy.

In this energy regime, the measured spectral spectrum of sample 1 exhibits high conversion efficiency in the plateau region (see Fig. 4(a); red (top) curve). However, no additional uv extension was observed, which means that uv cutoff is not further pushed to shorter wavelengths. As a result, the rising of the free-electron density does not increase the maximum positive frequency shift but significantly contributes to the enhancement of conversion efficiency of the continuum generation. These observations provide clear evidence that the uv cutoff is limited by clamping of the peak intensity inside the filaments [45,46]. Another minor deviation concerns the spectral modulations (fringe structure) that are seen in the spectrum, in particular, between 800 and 450 nm. At higher laser intensity, according to the moving-focus model the pulse develops a multipeaked structure. These subpulses generate continua via an on-axis phase retardation. This means that the observed continuum spectrum is the summation of the broadened spectra produced by each of these transient subpulses. Thus the observed spectral modulation can be seen as far-field interference resulting from the multiple broad bandwidth sources [47]. Our experimental data show that the pump pulse first undergoes a single splitting and then multiple splittings, in agreement with the theoretical prediction [18] of propagation dynamics of femtosecond laser pulses in a nonlinear medium.

IV. CONCLUSIONS

In summary, we have investigated the dynamics of ultrashort optical pulses propagating in transparent condensed media in direct time-domain. Our results indicate that the spatiotemporal modification of the pulse shape and the corresponding spectra broadening result from complex physical phenomena such as Kerr nonlinearity, plasma generation, group-velocity dispersion, diffraction, and self-steepening of the pulse fronts. In particular, in the regime where SF is balanced by free electrons, spectral broadening can result from four-wave mixing. We found that high conversion efficiency of the initial laser pulse to the supercontinuum is triggered by the occurrence of very strong SF and that MPI would be responsible for enhancing anti-Stokes broadening (positive frequency). The maximum blue shift of the spectrum remains constant for pulse energies above an input laser energy threshold. This is the evidence for the peak intensity clamping inside the filaments. For high pulse energy, we have shown that the propagation is characterized by the formation of multiple filaments, resulting from the interference of the ring system caused by the defocusing of light in the laser-produced plasma. Our experimental observations are in good agreement with previous simulation results.

ACKNOWLEDGMENTS

We gratefully acknowledge financial support from the Deutsch Forschungsgemeinschaft (SFB 613) and the discussion with N. Müller and W. Pfeiffer.

[1] R. R. Alfano, *The Supercontinuum Laser Source* (Springer-Verlag, NewYork, 1989).
[2] L. Sudrie, A. Couairon, M. Franco, B. Lamouroux, B. Prade, S. Tzortzakis, and A. Mysyrowicz, Phys. Rev. Lett. **89**, 186601 (2002).
[3] D. Faccio *et al.*, J. Opt. Soc. Am. B **22**, 862 (2005).
[4] V. V. Yakovlev *et al.*, Opt. Lett. **19**, 2000 (1994).
[5] C. P. Hauri *et al.*, Appl. Phys. B **79**, 673 (2004).
[6] L. Bergè and A. Couairon, Phys. Plasmas **7**, 210 (2000).
[7] J. Kasparian *et al.*, Science **301**, 61 (2003).
[8] I. Z. Kozma, P. Krok, and E. Riedle, J. Opt. Soc. Am. B **22**, 1479 (2005).
[9] G. Yang and Y. R. Shen, Opt. Lett. **9**, 510 (1984).
[10] M. Wittman and A. Penzkofer, Opt. Commun. **126**, 308 (1996).
[11] P. B. Corkum, C. Rolland, and T. Srinivasan-Rao, Phys. Rev. Lett. **57**, 2268 (1986).
[12] N. Bloembergen, Opt. Commun. **8**, 285 (1973).
[13] W. L. Smith, P. Liu, and N. Bloembergen, Phys. Rev. A **15**, 2396 (1977).
[14] A. Brodeur and S. L. Chin, J. Opt. Soc. Am. B **16**, 637 (1999).
[15] Yu. P. Raizer, Sov. Phys. Usp. **8**, 650 (1966).
[16] V. P. Kandidov *et al.*, Appl. Phys. B **77**, 149 (2003).
[17] J. E. Rothenberg, Opt. Lett. **17**, 1340 (1992).
[18] A. A. Zozulya, S. A. Diddams, A. G. Van Engen, and T. S. Clement, Phys. Rev. Lett. **82**, 1430 (1999).
[19] V. Tikhonenko, J. Christou, and B. Luther-Davies, Phys. Rev. Lett. **76**, 2698 (1996).
[20] D. M. Rayner, A. Naumov, and P. B. Corkum, Opt. Express **13**, 3208 (2005).
[21] S. L. Chin *et al.*, Can. J. Phys. **83**, 863 (2005).
[22] A. L. Gaeta, Phys. Rev. Lett. **84**, 3582 (2000).
[23] S. A. Akmanov, V. A. Vyslouh, and A. S. Chirkin, *Optics of Femtosecond Laser Pulses* (American Institute of Physics, New York, 1992).
[24] W. Liu, S. A. Hosseini, Q. Luo, B. Ferland, S. L. Chin, O. G. Kosareva, N. A. Panov, and V. P. Kandidov, New J. Phys. **6**, 6 (2004).
[25] S. L. Chin, S. Petit, W. Liu, A. Iwasaki, M.-C. Nadeau, V. P. Kandidov, O. G. Kosareva, and K. Yu. Andrianov, Opt. Commun. **210**, 329 (2002).

[26] J. Yang and G. Mu, Opt. Express **15**, 4943 (2007).
[27] A. Saliminia, S. L. Chin, and R. Vallée, Opt. Express **13**, 5731 (2005).
[28] H. Nishioka, W. Odajima, K. Ueda, and H. Takuma, Opt. Lett. **20**, 2505 (1995).
[29] H. Nishioka and K. Ueda, Appl. Phys. B **77**, 171 (2003).
[30] Q. Luo, S. A. Hosseini, B. Ferland, and S. L. Chin, Opt. Commun. **233**, 411 (2004).
[31] V. P. Kandidov, N. Aközbek, M. Scalora, O. G. Kosareva, A. V. Nyakk, Q. Luo, S. A. Hosseini, and S. L. Chin, Appl. Phys. B **80**, 267 (2005).
[32] S. A. Hosseini, Q. Luo, B. Ferland, W. Liu, S. L. Chin, O. G. Kosareva, N. A. Panov, N. Aközbek, and V. P. Kandidov, Phys. Rev. A **70**, 033802 (2004).
[33] H. Schroeder, J. Liu, and S. L. Chin, Opt. Express **12**, 4768 (2004).
[34] F. Quere', S. Guizard, and P. Martin, Europhys. Lett. **56**, 138 (2001).
[35] D. Faccio, A. Averchi, A. Lotti, M. Kolesik, J. V. Moloney, A. Couairon, and P. Di Trapani, Phys. Rev. A **78**, 033825 (2008).
[36] A. Brodeur and S. L. Chin, Phys. Rev. Lett. **80**, 4406 (1998).
[37] S. Tzortzakis, L. Sudrie, M. Franco, B. Prade, A. Mysyrowicz, A. Couairon, and L. Berge, Phys. Rev. Lett. **87**, 213902 (2001).
[38] Q. Xing, K. M. Yoo, and R. R. Alfano, Appl. Opt. **32**, 2087 (1993).
[39] O. G. Kosareva *et al.*, Opt. Lett. **22**, 1332 (1997).
[40] G. G. Luther *et al.*, Opt. Lett. **19**, 789 (1994).
[41] C. Nagura *et al.*, Appl. Opt. **41**, 3735 (2002).
[42] P Martin, S. Guizard, P. Daguzan, G. Petite, P. D'Oliveira, P. Meynadier, and M. Perdrix, Phys. Rev. B **55**, 5799 (1997).
[43] B. Rethfeld, K. Sokolowski-Tinten, D. Von Der Linde, and S. I. Anisimov, Appl. Phys. A **79**, 767 (2004).
[44] V. V. Temnov *et al.*, Phys. Rev. Lett. **97**, 237403 (2006).
[45] W. Liu *et al.*, Opt. Commun. **202**, 189 (2002).
[46] J. Kasparian, R. Sauerbrey, and S. L. Chin, Appl. Phys. B: Lasers Opt. **71**, 877 (2000).
[47] D. Strickland and P. B. Corkum, J. Opt. Soc. Am. B **11**, 492 (1994).